Neurobiology of Disease

Stroke Accelerates and Uncouples Intrinsic and Synaptic Excitability Maturation of Mouse Hippocampal DCX$^+$ Adult-Born Granule Cells

Mihai Ceanga,[1] Silke Keiner,[1] Benedikt Grünewald,[1,2] Holger Haselmann,[1,2] Christiane Frahm,[1] Sebastien Couillard-Després,[3] Otto W. Witte,[1] Christoph Redecker,[1] Christian Geis,[1] and Albrecht Kunze[1]

[1]Hans Berger Department of Neurology, [2]Integrated Research and Treatment Center—Center for Sepsis Control and Care (CSCC), Jena University Hospital, 07747 Jena, Germany, and [3]Institute of Experimental Neuroregeneration, Spinal Cord Injury and Tissue Regeneration Center Salzburg, Paracelsus Medical University, 5020 Salzburg, Austria

Stroke robustly stimulates adult neurogenesis in the hippocampal dentate gyrus. It is currently unknown whether this process induces beneficial or maladaptive effects, but morphological and behavioral studies have reported aberrant neurogenesis and impaired hippocampal-dependent memory following stroke. However, the intrinsic function and network incorporation of adult-born granule cells (ABGCs) after ischemia is unclear. Using patch-clamp electrophysiology, we evaluated doublecortin-positive (DCX$^+$) ABGCs as well as DCX$^-$ dentate gyrus granule cells 2 weeks after a stroke or sham operation in DCX/DsRed transgenic mice of either sex. The developmental status, intrinsic excitability, and synaptic excitability of ABGCs were accelerated following stroke, while dendritic morphology was not aberrant. Regression analysis revealed uncoupled development of intrinsic and network excitability, resulting in young, intrinsically hyperexcitable ABGCs receiving disproportionately large glutamatergic inputs. This aberrant functional maturation in the subgroup of ABGCs in the hippocampus may contribute to defective hippocampal function and increased seizure susceptibility following stroke.

Key words: **aberrant integration; adult neurogenesis; doublecortin; hyperexcitability; stroke; uncoupled maturation**

Significance Statement

Stroke increases hippocampal neurogenesis but the functional consequences of the postlesional response is mostly unclear. Our findings provide novel evidence of aberrant functional maturation of newly generated neurons following stroke. We demonstrate that stroke not only causes an accelerated maturation of the intrinsic and synaptic parameters of doublecortin-positive, new granule cells in the hippocampus, but that this accelerated development does not follow physiological dynamics due to uncoupled intrinsic and synaptic maturation. Hyperexcitable immature neurons may contribute to disrupted network integration following stroke.

Introduction

In the adult dentate gyrus, new granule neurons develop continually from a local population of neural progenitor cells and integrate in the preexisting network, modulating its plasticity and function (van Praag et al., 2002; Schmidt-Hieber et al., 2004; Nakashiba et al., 2012; Ikrar et al., 2013; Adlaf et al., 2017). The process of adult neurogenesis is influenced by environmental factors such as learning, running, and enriched environment (Kempermann et al., 1997; van Praag et al., 1999; Couillard-Després et al., 2005; Ambrogini et al., 2010; Nokia et al., 2012; Bergami et al., 2015), but also by disease, including stroke, epilepsy, trauma, and inflammation, as well as by aging (Liu et al., 1998; Kluska et al., 2005; Jessberger et al., 2007; Jakubs et al., 2008; Walter et al., 2011; Chugh et al., 2013; Couillard-Després, 2013; Villasana et al., 2015). Stroke has a high prevalence in developed countries and is

Received Nov. 20, 2017; revised Nov. 5, 2018; accepted Nov. 8, 2018.

Author contributions: M.C., S.K., S.C.-D., C.R., C.G., and A.K. designed research; M.C., S.K., B.G., and C.F. performed research; M.C., S.K., B.G., H.H., C.F., O.W.W., C.R., C.G., and A.K. analyzed data; M.C., S.K., B.G., H.H., O.W.W., C.R., C.G., and A.K. wrote the paper.

This work was supported by the Interdisciplinary Center for Clinical Research Jena (to M.C. and Project FF06 to S.K.), the German Ministry of Education and Research (BMBF program "Cell-based, regenerative therapies," Grant 01GN0977 to C.R.), the Deutsche Forschungsgemeinschaft (CRC-TR 166 [TP B2 to C.G. GE2519_3-1 to C.G., and KE 1914/2-1 to S.K.). We thank Julia Karius, Madlen Günther, and Ina Ingrisch for technical assistance, as well as Marc Raugust and Maximilian Jamin for immunocytochemical image acquisition and analysis. We also thank Dr. Thomas Lehmann (Jena University Hospital) for help with the statistical analysis of the data.

The authors declare no competing financial interests.

Correspondence should be addressed to Albrecht Kunze at albrecht.kunze@med.uni-jena.de.

https://doi.org/10.1523/JNEUROSCI.3303-17.2018

 0270-6474/19/391755-12$15.00/0

a significant burden on the quality of life of afflicted individuals. Although cognitive disturbances and depression are frequent complications, the mechanisms of these secondary neuropsychiatric disorders are not fully understood (Wang et al., 2010; Loubinoux et al., 2012; Robinson and Jorge, 2016; Mijajlovic et al., 2017).

Stroke induces remote effects such as strongly stimulating the proliferation and differentiation of neurogenic precursor cells in the hippocampus (Liu et al., 1998; Arvidsson et al., 2001), even as the dentate gyrus is not directly affected. Despite the increased number of adult-born granule cells (ABGCs) following stroke, there is a higher incidence of abnormalities in the migration and morphology of these cells (Niv et al., 2012; Woitke et al., 2017) and affected mice show deficits in hippocampal-dependent memory tasks (Woitke et al., 2017). Moreover, stimulating neurogenesis through a running paradigm after stroke provides even more ABGCs, but paradoxically accentuates hippocampus-dependent memory deficits (Woitke et al., 2017). However, electrophysiological data of ABGCs after stroke are lacking, and it is unknown whether ABGCs poststroke undergo changes in excitability and network integration.

The migration-associated protein doublecortin (DCX) is expressed by immature neurons approximately up to the fourth week postmitosis, when cellular migration, maturation of intrinsic excitability, and synaptic integration take place (Brown et al., 2003; Zhao et al., 2008; Jagasia et al., 2009). We investigated DCX-positive (DCX^+) as well as DCX-negative (DCX^-) neurons in a transgenic mouse line expressing the red fluorescent protein (RFP) DsRed under control of the *DCX* promoter (Karl et al., 2005; Couillard-Després et al., 2006) to explore the impact of experimental ischemic stroke on neuronal intrinsic excitability and synaptic function. We found an accelerated maturation of both intrinsic and network excitability of DCX^+ neurons after middle cerebral artery occlusion (MCAO), while the dendritic morphology of these neurons was unchanged to sham DCX^+ neurons. Importantly, we found that intrinsic and network maturation are tightly coupled under normal conditions but are disrupted after stroke, resulting in intrinsically hyperexcitable ABGCs that additionally receive even stronger synaptic inputs. While we presently cannot rule out that increased excitability is a consequence rather than a cause of hippocampal dysfunction, we provide new data on disrupted integration of ABGCs in the hippocampus following stroke.

Materials and Methods

All experimental procedures were in accordance with the European Directives and were approved by the German Animal Care and Use Committee. Mice of either sex were used in all experiments.

Middle cerebral artery occlusion procedure. *DCX*/DsRed mice (Couillard-Després et al., 2006) received a 45 min middle cerebral artery occlusion or a sham operation at 3 months of age (14 sham mice, 30 mice with MCAO as previously described; Niv et al., 2012). Briefly, the common carotid artery was exposed and ligated on the right side under ~2.5% isoflurane (CP Pharma) anesthesia. A 3.0 monofilament suture (Doccol; RRID: SCR_015960) with a rounded tip was inserted into the common carotid artery after arteriotomy and advanced to occlude the middle cerebral artery. The suture was removed after 45 min, the wound was closed, and the animals were allowed to recover. Sham-operated animals underwent the same treatment without occlusion of the right internal carotid artery. Of the 30 animals that received an MCAO, 6 died, 1 was excluded due to affection of the hippocampus, and 2 were excluded due to a nonvisible fluorescent signal in the dentate gyrus. The sexes of the animals used were as follows: 9 males (64%) and 5 females (36%) in the sham group and 11 males (52%) and 10 females (48%) in the MCAO group.

In vitro *electrophysiology.* Two weeks after the sham/MCAO procedure, the animals were killed after isoflurane anesthesia, and 300-μm-thick transverse slices were prepared on a vibratome from the ipsilateral hippocampus (VT 1200S, Leica) in sucrose-based solution containing the following (in mM): 87 NaCl, 25 $NaHCO_3$, 2.5 KCl, 1.25 NaH_2PO_4, 0.5 $CaCl_2$, 7 $MgCl_2$, 25 glucose, 75 sucrose, and 1.3 ascorbate (Sigma-Aldrich). Slices were incubated for 45 min at 33°C in aCSF containing the following (in mM): 126 NaCl, 26 $NaHCO_3$, 3 KCl, 1.25 NaH_2PO_4, 2 $CaCl_2$, 1 $MgSO_4$ (Sigma-Aldrich), 10 glucose, and 1.3 ascorbate (osmolarity, 310 mOsm/kg) before allowing recovery in aCSF at room temperature for at least 1 h. Patch pipettes were pulled using a P-87 horizontal pipette puller (Sutter Instruments) from borosilicate glass (0.86 × 1.50; Science Products) and had a resistance of 3–7 MΩ when filled with an intracellular solution containing the following (in mM): 140 potassium-gluconate, 10 NaCl, 2 MgATP (Sigma-Aldrich), 0.3 NaGTP (Sigma-Aldrich), 0.6 EGTA (Sigma-Aldrich), 10 HEPES, and 3 mg/ml biocytin (Tocris Bioscience; pH 7.2 with KOH; osmolarity, 285 mOsm/kg). All chemicals were purchased from Carl Roth unless stated otherwise.

Granule cells were visually identified using a microscope (Examiner.Z1, Zeiss) equipped with differential interference contrast optics. Neurons were recorded predominantly from the ventral pole of the hippocampus. DCX^+ cells were identified under fluorescent illumination (HXP 120 C, LEJ) and fluorescent filling of the pipette tip during tight sealing was photographically documented and used to confirm the identity of recorded cells. Voltage-clamp and current-clamp signals were recorded with an Axopatch 200B Amplifier (Molecular Devices), filtered at 2 or 5 kHz, and digitized using a Digidata 1440A digitizer (Molecular Devices) at 10 or 25 kHz, respectively. Data acquisition was performed in Clampex 10.5, and the analysis was performed in Clampfit 10.5 (Molecular Devices). Seal resistance was at least three to five times the input resistance (R_{input}). Measured voltages were corrected off-line for a 12 mV, experimentally determined, liquid junction potential. Access resistance (R_a; up to 50 MΩ, not compensated) was monitored throughout the experiment, and recordings were discarded if deviations of >20% occurred. Recordings were made at room temperature under an aCSF flow of 2 ml/min (Ismatec). Voltage-clamp measurements were performed at a (corrected) holding value of −82 mV. Resting potential (V_{rest}) was determined immediately after obtaining whole-cell configuration. Higher R_a can cause an error in the measurement of V_{rest}, especially in young, small, and depolarized ABGCs. However, there was no statistical difference in R_a values among sham DCX^+ and MCAO DCX^+ neurons ($n = 33$ sham DCX^+ cells and $n = 43$ MCAO DCX^+ cells; $p = 0.086$, Mann–Whitney $U = 306$). Membrane capacitance (C_m) was determined after fitting a two-term exponential function on the current transients in response to a hyperpolarizing 5 mV voltage step according to the following formulae:

$$\tau_w = \frac{\tau_1 \cdot A_1 + \tau_2 \cdot A_2}{A_1 + A_2}$$

$$C_m = \tau_w \frac{R_{input} + R_a}{R_{input} \cdot R_a}.$$

Action potentials (APs) were elicited by an incrementing series of depolarizing current injections (300 ms) starting from a holding current of 0 pA (at resting membrane potential). The amplitude of the injected current was adapted to the passive properties of the measured cell. In a separate protocol and to determine whether a cell would change AP configuration after hyperpolarization, a ramp current brought the cell from approximately −100 to +50 mV. While this sometimes slightly increased spikelet amplitude in immature neurons, it did not change the configuration of the response or the pattern of discharge. AP threshold was defined as the potential at which the rise slope of the AP exceeded 15 V/s. AP amplitude was measured respective to the resting membrane potential.

Spontaneous EPSCs (sEPSC) and miniature EPSC (mEPSC) were measured in the presence of 10 μM picrotoxin (PTX; Sigma-Aldrich), or 10 μM PTX and 1 μM tetrodotoxin (TTX; Sigma-Aldrich), respectively. Analysis of synaptic currents was performed in Clampfit 10.5 using the

template search function. Templates of sEPSC and mEPSC were obtained by averaging 25–35 manually selected events per group. All events with a similarity threshold of four were user reviewed and manually confirmed.

Stimulation of the lateral perforant path (LPP) was performed with an aCSF-filled patch pipette acting as a monopolar stimulation electrode, which was lowered into the outer third of the molecular layer ~200–300 μm from the recording electrode. Stimulation was applied through a constant current stimulation unit (DS3, Digitimer) at 0.1 Hz for 40 μs. Stimulation intensity (10–100 μA) was adjusted to produce half-maximal (40–60%) responses. Paired-pulse stimulation was applied at 100 ms intervals at 0.1 Hz.

Biocytin staining and morphologic analysis. After recording, slices were transferred in 4% paraformaldehyde (PFA) and fixed overnight at 4°C. After washing in TBS, slices were incubated for 2 h in TBS plus (TBS, 5% donkey serum, 0.3% Triton X-100) and then incubated overnight in 1:500 streptavidin-Cy3 (Sigma-Aldrich) in TBS plus before embedding in Entellan (Merck). Filled neurons were captured on a confocal scanning microscope (LSM 710, Zeiss), and morphologic analysis was performed in Imaris (Bitplane).

Birth tracing and immunocytochemistry. Bromodeoxyuridine (BrdU) labeling of proliferating cells was performed in three sham and five MCAO mice. After the sham/MCAO procedure, BrdU (Sigma-Aldrich) was applied intraperitoneally every 12 h at a dose of 50 mg/kg for 2 weeks. Thereafter, the animals were deeply anesthetized with isoflurane and perfused through the ascending aorta with 4% PFA in phosphate buffer (0.15 mol/L, pH 7.4). The brains were removed and sliced into 40 μm sections. The following primary and secondary antibodies were used: rat anti-BrdU antibody (1:500 overnight; catalog #OBT0030CX, Bio-Rad; RRID:AB_609566), rabbit anti-RFP antibody (1:500 overnight; catalog #ab62341, Abcam; RRID:AB_945213), Alexa Fluor 488 anti-rat (1:500, 3 h at RT; catalog #A11006, Thermo Fisher Scientific; RRID: AB_2534074), Rhodamine Red anti-rabbit (1:500, 3 h at RT; catalog #711-297-003, Jackson ImmunoResearch; RRID:AB_2340615). Immunofluorescence stainings were analyzed by confocal laser scanning microscopy (LSM 710, Zeiss). Fifty BrdU-positive ($BrdU^+$) cells per mouse (only ipsilateral hemispheres were used) were randomly selected and assessed for RFP coexpression, and another 50 RFP-positive (RFP^+) cells were analyzed for BrdU coexpression.

Experimental design and statistical analysis. The researcher performing the experiments was blinded to the treatment of the animal. Statistical analysis and graphical representations were performed in SPSS 21 (IBM) and MS-Excel (Microsoft). The statistical unit was the cell (except in the analysis of immunocytochemical data, where it is the number of mice), and the number of cells (n) per group is mentioned in the text and figures (or corresponding legend), while both n and the number of mice (N) from which the respective cells were collected are mentioned in the tables. A normal distribution was excluded using the Shapiro–Wilk test in all recorded parameters, except for AP threshold ($p = 0.496$) and total dendritic length (TDL; $p = 0.116$). Consequently, between-group comparisons were performed using nonparametric tests (Mann–Whitney test for two-group comparisons), and central tendencies were reported as the median and interquartile range (IQR). The α was set at 0.05. Correction for multiple comparisons was performed by the false discovery rate Benjamini–Hochberg procedure with a Q set at 5%, $m = 41$ and 32 in a second set of experiments (Benjamini et al., 2001). This translated into significant p values, which are <0.04. Statistical analysis of current–frequency curves was performed using mixed linear models in SPSS. Covariation of R_{input}, mEPSC amplitude and output gain, as well as maximal AP rise slope and TDL was performed using the general linear model (GLM). When the data were nonlinearly distributed, we used the logarithmic transform instead (which was normally distributed in the Shapiro–Wilk test).

Results

Stroke accelerates cellular maturation of DCX^+ ABGCs

We performed whole-cell patch-clamp recordings of randomly selected DCX^+ immature neurons in the inner layer of the dentate gyrus of the ipsilateral hippocampus 2 weeks after MCAO. Fluorescent signal in the pipette tip in on-cell configuration was used to confirm the identity of recorded cells (Fig. 1*A*). DCX-negative (DCX^-) neurons in the middle and outer third of the granule cell layer were also recorded, representing mature cells or cells in advanced stages of maturation and integration. Numerical values are reported as the median and IQR unless stated otherwise.

R_{input} is known to be inversely correlated with cell maturation (Liu et al., 2000; Schmidt-Hieber et al., 2004; Ye et al., 2005; Couillard-Després et al., 2006; Schmidt-Salzmann et al., 2014). R_{input} was predictably low in sham DCX^- neurons and high in sham DCX^+ cells (0.55 GΩ; IQR, 0.29; $n = 18$; and 3.5 GΩ; IQR, 4.0; $n = 33$, respectively). After MCAO, R_{input} more than halved in DCX^+ neurons to 1.55 (IQR, 2.69; Fig. 1*B–D*, Table 1; $n = 43$; Mann–Whitney $U = 418$, $p = 0.002$ vs sham DCX^+). Classifying neurons by R_{input} into mature ($R_{input} \leq 0.5$ GΩ), intermediate ($0.5 < R_{input} < 1$ GΩ), and immature ($R_{input} \geq 1$ GΩ; Fig. 1*C*, Table 1) showed a significant shift of MCAO DCX^+ neurons toward more advanced maturation stages ($n = 76$, $p = 0.025$, Mann–Whitney $U = 569$). Furthermore, accelerated maturation in MCAO DCX^+ granule cells was also observed by a decrease in their V_{rest} and membrane time constant (τ_m; Fig. 1*E,F*) and an increase in C_m (Table 1). This response was specific for DCX^+ neurons, since stroke altered cellular properties of resident, DCX^- neurons in the opposite direction, increasing R_{input} and V_{rest}, while leaving τ_m unaffected (Fig. 1*B–F*, Table 1). Thus, MCAO differentially affects the electrotonic properties of dentate granule cells, with a maturation shift in DCX^+ ABGCs.

Stroke accelerates action potential maturation in DCX^+ ABGCs

Next, we investigated the influence of ischemic stroke on AP generation of DCX^+ ABGCs. The voltage responses of all granule cells to incremental injections of current can be categorized into three groups based on the maximal rate of AP rise (Fig. 2*A*). According to previously published criteria (Schmidt-Salzmann et al., 2014), mature APs were defined as APs with rise slopes of $\geq$300 V/s while immature APs had rise slopes of $\leq$100 V/s. Cells with values in between were classified as having intermediate APs. Sham DCX^- neurons responded with sustained trains of mature APs (maximal rise, 390 V/s; IQR, 64.7; $n = 18$; Fig. 2*B–D*, Table 2). Only 1 of 18 sham DCX^- cells showed an intermediate AP phenotype. On the other hand, sham DCX^+ ABGCs had much lower rates of rise of 10.5 V/s (IQR, 213.8; $n = 30$; Fig. 2*B–D*, Table 2), in accordance with previous reports (Schmidt-Hieber et al., 2004; Spampanato et al., 2012; Schmidt-Salzmann et al., 2014). Most DCX^+ ABGCs (21 of 30 cells) fired nonovershooting, slow, and broad immature APs, while 5 of 30 fired intermediate APs, and only 4 of 30 fired brisk, mature APs (Fig. 2*B–D*, Table 2). In stark contrast, APs of DCX^+ ABGCs had significantly faster rise slopes after MCAO (186.7 V/s; IQR, 341.4; $n = 41$; Mann–Whitney $U = 365$, $p = 0.004$ vs sham DCX^+) and included a substantial subset of cells with mature APs (17 of 41 APs; Fig. 2*B, C*, Table 2). As in the case of passive properties, there was a significant shift toward more mature APs following MCAO in DCX^+ ABGCs (Fig. 2*C*, Table 2; $n = 71$; Mann–Whitney $U = 398$, $p = 0.005$). However, compared with DCX^- neurons without stroke, no changes were seen in the AP properties of resident DCX^- neurons after MCAO (Fig. 2*B–D*, Table 2). Associated with the faster AP kinetics, maximal inward currents in response to step depolarizations were greater in DCX^+ ABGCs after MCAO (Table 2; 2.93 nA; IQR, 4.92; $n = 43$ vs 0.47 nA; IQR, 3.13; $n = 20$, Mann–Whitney $U = 271$, $p = 0.019$, in MCAO DCX^+ and sham DCX^+ cells, respectively). Repolarization dynamics, as

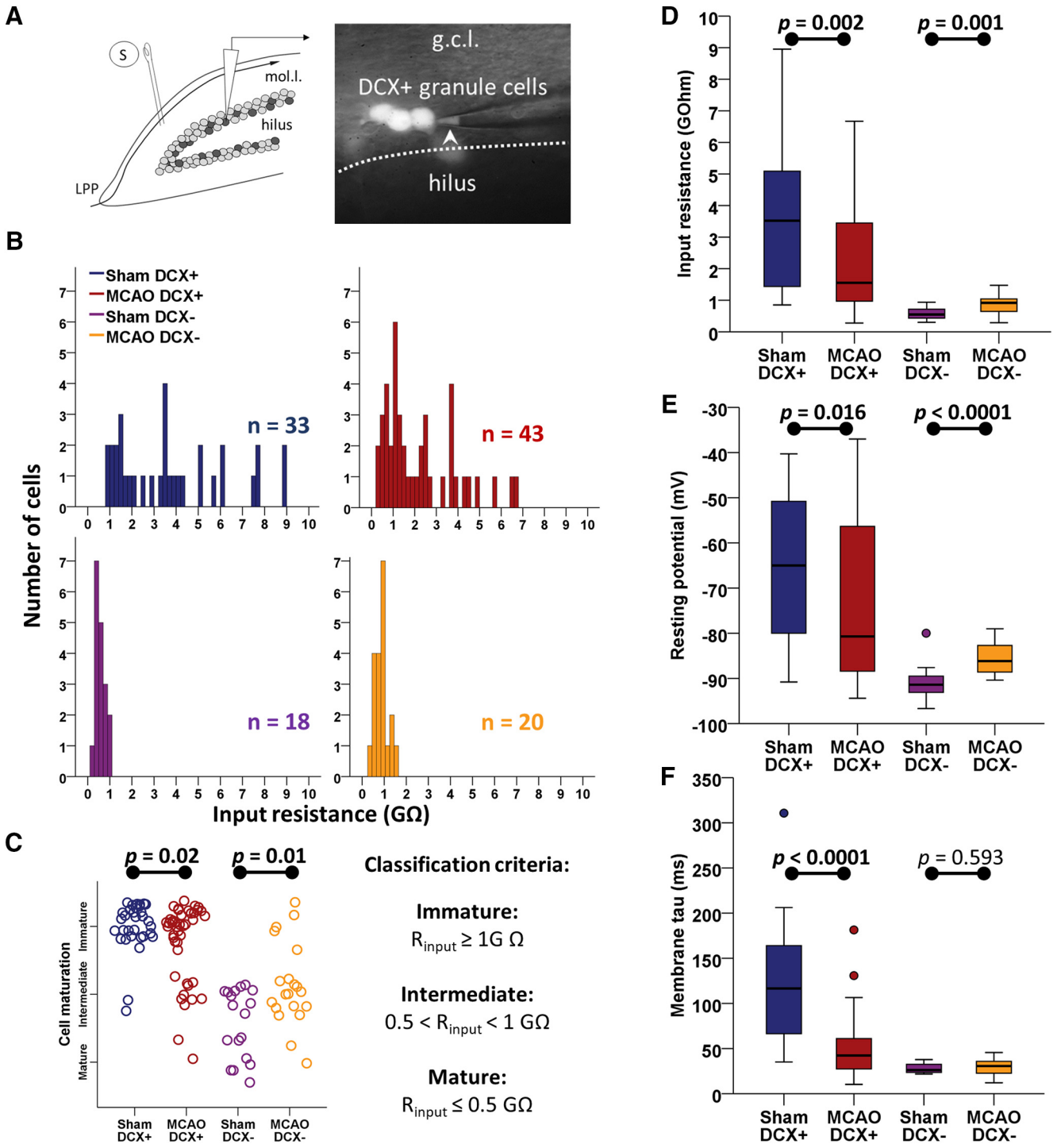

Figure 1. Stroke accelerates cellular maturation of DCX$^+$ ABGCs. ***A***, Schematic illustration of the recording configuration in the granule cell layer of the dentate gyrus. DCX$^+$ phenotype of recorded cells was confirmed by the presence of fluorescence signal in the pipette tip in on-cell configuration (arrowhead). S, Stimulation electrode; mol.l., molecular layer; g.c.l., granule cell layer. ***B***, Histograms of R_{input} in the studied population of sham DCX$^+$ ($n = 33$), MCAO DCX$^+$ ($n = 43$), sham DCX$^-$ ($n = 18$), and MCAO DCX$^-$ ($n = 20$) cells. The distribution of R_{input} in the MCAO DCX$^+$ group is shifted to the left, indicating a more mature phenotype, while in the MCAO DCX$^-$ group it is shifted to the right, indicating that stroke has selective effects on different cell subpopulations. ***C***, Distribution of cells within the groups of mature, intermediate, and immature cells (right, definitions) shows a shift toward a more mature phenotype in DCX$^+$ neurons after MCAO, while MCAO DCX$^-$ neurons are differently affected. ***D***, Comparative boxplot distribution of R_{input} in the four groups shows a significant decrease (more than half) in DCX$^+$ neurons after stroke. ***E***, ***F***, Resting membrane potential (***E***) and membrane tau (***F***) also show subpopulation-specific modifications after MCAO, with a maturation shift in DCX$^+$ neurons. See also Table 1 for statistical results.

measured by the rise/decay ratio, were also altered in DCX$^+$ ABGCs following MCAO (Table 2). In conclusion, cerebral ischemia speeds up the maturation of DCX$^+$ ABGCs also with respect to their intrinsic excitability and AP generation, while leaving DCX$^-$ neurons unaffected.

DCX$^+$ ABGCs with mature APs remain hyperexcitable after stroke

DCX$^+$ neurons are known to be intrinsically hyperexcitable (Mongiat et al., 2009). As shown above, the proportion of DCX$^+$ neurons producing mature APs is higher after MCAO, yet

Table 1. Passive, electrotonic properties of hippocampal granule cells

	Sham DCX$^+$		Sham DCX$^-$		MCAO DCX$^+$		MCAO DCX$^-$		M-W *U* test Sham DCX$^+$ vs MCAO DCX$^+$			M-W *U* test Sham DCX$^-$ vs MCAO DCX$^-$		
Passive properties	*n*/*N*	Median (IQR)	*n*/*N*	Median (IQR)	*n*/*N*	Median (IQR)	*n*/*N*	Median (IQR)	*p*	*U*	η^2	*p*	*U*	η^2
V_{rest} (mV)	33/11	−65 (31.1)	18/9	−91.4 (3.7)	43/17	−80.7 (32.7)	20/5	−86.2 (6.1)	0.016	480.5	7.7%	<0.0001	36	47.9%
R_{input} (GΩ)	33/11	3.52 (4.0)	18/9	0.55 (0.29)	43/17	1.56 (2.7)	20/5	0.92 (0.4)	0.002	418	12.4%	0.001	66	30.0%
C_m (pF)	33/11	5.5 (17.2)	18/9	36.8 (32.6)	43/17	19.3 (22.5)	19/5	59.0 (31.3)	0.025	496	6.7%	0.004	77	22.7%
τ_m (ms)	30/11	116.5 (100.2)	18/9	26.3 (9.4)	41/17	42.8 (34.6)	20/5	30.6 (13.9)	<0.0001	176	37.3%	0.593	161	0.8%
Cell maturation	33/11	Fraction (%)	18/9	Fraction (%)	43/17	Fraction (%)	20/5	Fraction (%)	0.025	569	6.8%	0.010	93	23.1%
Immature		31/33 (94%)		0/18 (0%)		32/43 (74%)		5/20 (25%)						
Intermediate		2/33 (6%)		10/18 (56%)		9/43 (21%)		13/20 (65%)						
Mature		0/33 (0%)		8/18 (44%)		2/43 (5%)		2/20 (10%)						

M-W, Mann–Whitney; *n*/*N*–, number of cells/number of mice. Summary of electrotonic cell properties in the three recorded groups. Resting potential was determined immediately after whole-cell access. Cell maturation group was defined based on input resistance as follows: immature cells had R_{input} of ≥1 GΩ, intermediately mature cells had a R_{input} <1 GΩ but >0.5 GΩ, and mature cells had an R_{input} of ≤0.5 GΩ. The statistical unit is *n*.

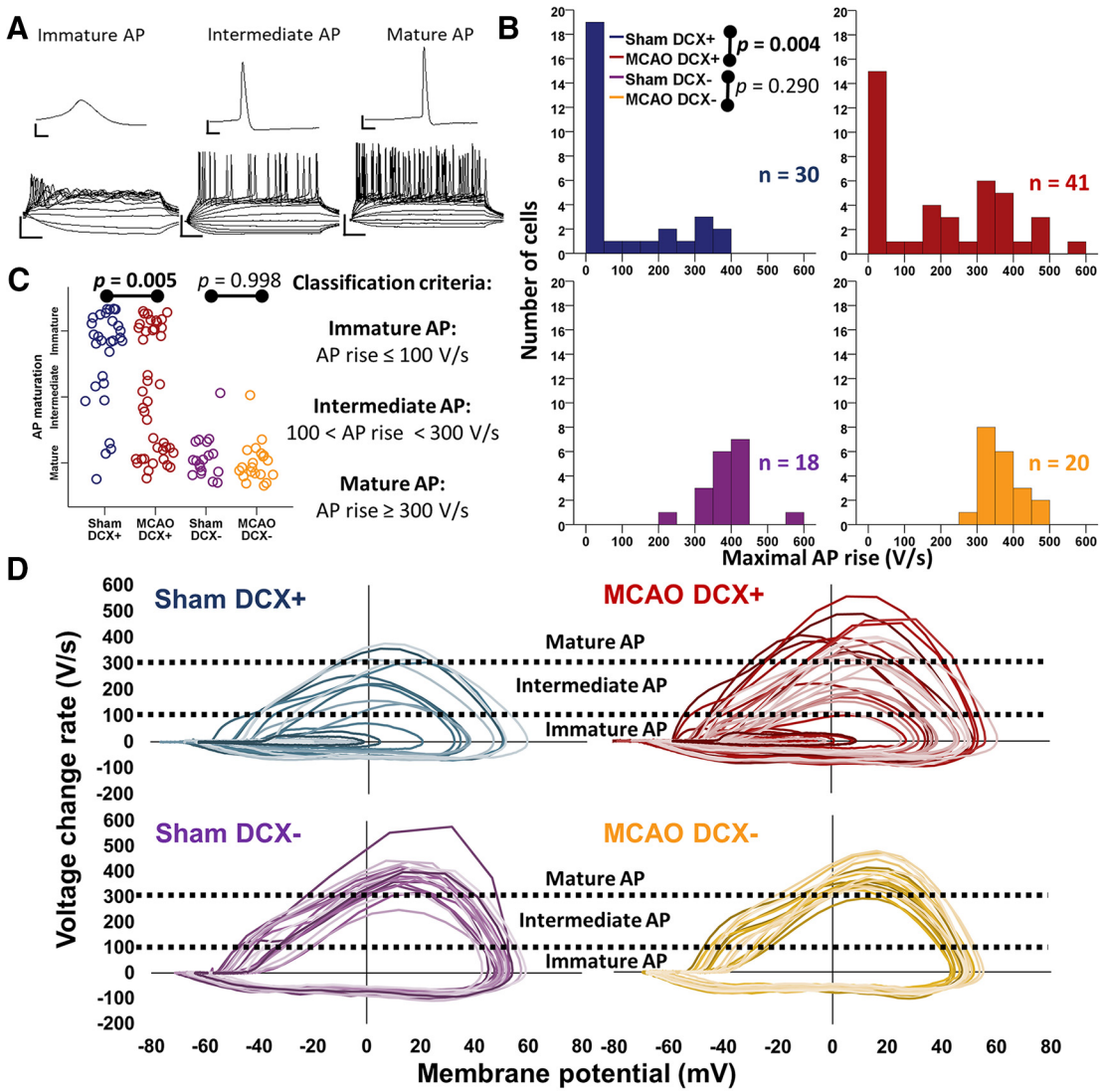

Figure 2. Stroke accelerates action potential maturation in DCX$^+$ ABGCs. ***A***, Representative voltage responses of granule cells to 300 ms stepwise current injections (calibration: top, 5 ms, 20 mV; bottom, 50 ms, 40 mV). ***B***, Histograms of maximal AP rise show faster APs after MCAO in DCX$^+$ ABGCs, but no change in DCX$^-$ neurons after stroke. ***C***, Based on maximal AP rise, cells could be classified into the following three groups: immature, intermediate, and mature APs (right, classification criteria). There was a higher proportion of mature APs after MCAO in DCX$^+$ neurons, but the distributions did not change after MCAO. ***D***, Phase plots of action potentials of all cells in the examined groups. Each trace represents one cell. Dashed horizontal lines represent the limits of immature, intermediate and mature AP (see above). See also Table 2 for statistical results.

whether these cells retain their intrinsic hyperexcitability characteristic of DCX$^+$ cells or mature to a lower intrinsic excitability characteristic of DCX$^-$ neurons is not known. We therefore investigated the excitability of DCX$^+$ cells generating mature APs compared with DCX$^-$ neurons. Only a minority of sham DCX$^+$ cells fulfilled the criteria of mature APs (4 of 30 APs), similar to previous studies (Spampanato et al., 2012; Schmidt-Salzmann et al., 2014). We found several significant differences between

Table 2. Intrinsic excitability of hippocampal granule cells

	Sham DCX$^+$		Sham DCX$^-$		MCAO DCX$^+$		MCAO DCX$^-$		M-W *U* test Sham DCX$^+$ vs MCAO DCX$^+$			M-W *U* test Sham DCX$^-$ vs MCAO DCX$^-$		
Intrinsic excitability	*n/N*	Median (IQR)	*n/N*	Median (IQR)	*n/N*	Median (IQR)	*n/N*	Median (IQR)	*p*	*U*	η^2	*p*	*U*	η^2
Max. inward current (nA)	20/10	−0.47 (3.13)	18/9	−6.61 (4.34)	43/17	−2.93 (4.92)	17/20	−8.10 (2.60)	0.019	271	8.9%	0.318	122	3.1%
Max. AP rise (V/s)	30/11	10.5 (213.8)	18/9	390.0 (64.7)	41/1–7	186.7 (341.4)	20/5	353.0 (68.2)	0.004	365	12.1%	0.290	143	3.2%
Max. AP decay (V/s)	30/11	−6.9 (54.5)	18/9	−86.0 (15.0)	41/17	−54.3 (61.8)	20/5	−81.4 (9.7)	0.007	383	10.4%	0.041	110	11.3%
AP rise/decay ratio	30/11	1.9 (2.2)	18/9	4.3 (1.3)	41/17	3.4 (3.0)	20/5	4.5 (1.5)	0.013	401.5	8.8%	0.613	162.5	0.7%
AP maturation group	30/11	Fraction (%)	18/9	Fraction (%)	41/17	Fraction (%)	20/5	Fraction (%)	0.005	398	11.0%	0.988	179	0.0%
Immature AP		21/30 (70%)		0/18 (0%)		16/41 (39%)		0/20 (0%)						
Intermediate AP		5/30 (17%)		1/18 (6%)		8/41 (20%)		1/20 (5%)						
Mature AP		4/30 (13%)		17/18 (94%)		17/41 (41%)		19/20 (95%)						
In cells with mature AP														
AP threshold (mV)	4/3	−47.2 (11.8)	17/8	−47.2 (8.9)	17/13	−46.0 (7.6)	19/5	−42.5 (9.3)	0.965	33	0.0%	0.066	103	9.8%
AP amplitude (mV)	4/3	132.2 (18.6)	17/8	140.6 (9.8)	17/13	133.6 (10.9)	19/5	133.6 (10.4)	0.965	33	0.0%	0.087	107	8.5%
Rheobase (pA)	4/3	30 (11)	17/8	50 (23)	15/12	30 (24)	19/5	40 (20)	0.736	26	0.9%	0.208	121	5.0%
Gain (Hz/pA)	4/3	0.39 (0.8)	17/8	0.26 (0.14)	15/12	0.46 (0.48)	19/5	0.24 (0.10)	0.885	28.5	0.1%	0.271	126.5	3.5%

M-W, Mann–Whitney; *n/N* = number of cells/number of mice. The maximal inward current was measured after incremental membrane potential depolarizations in voltage clamp mode. AP maturation was defined as follows: immature APs had maximal rise slopes of ≤100 V/s, intermediate APs had maximal rise slopes >100 V/s and <300 V/s, while mature AP had maximal rise slopes ≥300 V/s. The gain is the mean slope of *I–V* curves. The statistical unit is *n*.

DCX$^+$ and DCX$^-$ cells. The rheobase of both sham DCX$^+$ and MCAO DCX$^+$ ABGCs was reduced compared with their DCX$^-$ counterparts (Fig. 3*A*; 30 pA; IQR, 11; $n = 4$ vs 50 pA,; IQR, 23; $n = 17$; Mann–Whitney $U = 5.5$, $p = 0.006$ in sham DCX$^+$ and sham DCX$^-$, respectively; and 30 pA; IQR, 24; $n = 17$ vs 40 pA; IQR, 20; $n = 19$; Mann–Whitney $U = 78.5$, $p = 0.025$ in MCAO DCX$^+$ and MCAO DCX$^-$, respectively). Furthermore, the mean output gain (mean slope of current–frequency curves) of MCAO DCX$^+$ ABGCs (0.46 Hz/pA; IQR, 0.48; $n = 17$) was significantly higher than that of both sham DCX$^-$ cells (0.26 Hz/pA; IQR, 0.14; $n = 17$; Mann–Whitney $U = 61$, $p = 0.011$) and that of MCAO DCX$^-$ neurons (Fig. 3*B*; 0.24 Hz/pA; IQR, 0.10; $n = 19$; Mann–Whitney $U = 59$, $p = 0.003$). We did not see a statistical difference in the mean output gain of sham DCX$^+$ and sham DCX$^-$ neurons, but that is probably due to the expected low number of neurons with mature APs in the sham DCX$^+$ group. Furthermore, there were no differences in rheobase or output gain between sham and MCAO cells within the DCX$^+$ group or within the DCX$^-$ group (Fig. 3*A*,*B*, Table 2), indicating a similar level of excitability within these two cell populations.

We expanded the analysis to individual current traces by analyzing the effect of treatment on mean instantaneous frequency and the number of APs when controlling for injected current by means of mixed linear models (Fig. 3*C*,*D*). MCAO DCX$^+$ ABGCs had both a higher frequency and AP number output than MCAO DCX$^-$ cells (effect size (β) = 0.081; SE(β) = 0.009; $t = 8.764$, $p < 0.0001$; and $\beta = 0.007$, SE(β) = 0.003; $t = 2.796$, $p = 0.005$, respectively). Sham DCX$^+$ ABGCs had even lower-frequency outputs, but similar AP number output, compared with MCAO DCX$^+$ ABGCs ($\beta = -0.072$; SE(β) = 0.02; $t = -3.587$, $p = 0.0004$; and $\beta = 0.006$; SE(β) = 0.004; $t = 1.394$, $p = 0.165$, respectively), while sham DCX$^-$ cells had a similar output frequency and a slightly higher AP number output than MCAO DCX$^-$ cells ($\beta = 0.003$; SE(β) = 0.008; $t = 0.341$, $p = 0.733$ and $\beta = 0.008$; SE(β) = 0.002; $t = 3.676$, $p = 0.0003$, respectively). There was no difference between sham DCX$^+$ and sham DCX$^-$ cells in either frequency (Fig. 3*C*; $\beta = 0.006$; SE(β) = 0.012; $t = 0.506$, $p = 0.613$) or AP number output (Fig. 3*D*; $\beta = 0.005$; SE(β) = 0.003; $t = 1.474$, $p = 0.142$), again probably due to the low number of sham DCX$^+$ ABGCs with mature APs.

Together, DCX$^+$ ABGCs with mature APs are both more numerous following stroke and also continue to express features of hyperexcitability characteristic of DCX$^+$ neurons (a lower rheobase, higher mean output gain, steeper current–frequency curves, and an output of more APs) relative to DCX$^-$ cells.

Coordinated morphofunctional development of DCX$^+$ cells is maintained after stroke

Since the electrophysiological properties of DCX$^+$ neurons were profoundly affected after cerebral ischemia, we performed biocytin stainings of recorded neurons to investigate neuronal morphology. Mature DCX$^-$ neurons show an extensive, wide, and complex dendritic tree, reaching the outer edge of the molecular layer (Fig. 4*A*). Cellular morphology parallels electrophysiological development (Liu et al., 2000), such as AP maturation, by lengthening of the dendritic tree and invasion of the outer parts of the molecular layer. Accordingly, we found small dendritic branches reaching little outside the granule cell layer in cells with immature APs and more widely branched dendritic trees in DCX$^+$ ABGCs with intermediate and mature action potentials (Fig. 4*B*,*C*). When quantified by Sholl analysis, the TDL in sham DCX$^+$ ABGCs (Fig. 4*D*; 718 μm; IQR, 1194; $n = 7$) was not significantly altered after MCAO (1277 μm; IQR, 736; $n = 6$; Mann–Whitney $U = 12$, $p = 0.234$). Importantly, applying a general linear model to the parameters of maximal AP rise and TDL (Fig. 4*E*), we found a good correlation in both sham DCX$^+$ ($R^2 = 0.89$) and MCAO DCX$^+$ ABGCs ($R^2 = 0.86$), reflecting a conserved, coordinated morphofunctional development of ABGCs after MCAO. Thus, under pathological conditions of ischemia, normal neuronal morphology does not preclude disturbances of intrinsic excitability.

To determine the origin of DCX$^+$ cells relative to the induction of stroke, we performed birth tracing by labeling ABGCs with BrdU twice daily for 2 weeks following ischemia. We determined the colocalization of BrdU and RFP as a surrogate for DCX, since RFP expression is under the control of the *DCX* promoter. We found that in both the sham and MCAO groups, >60% of RFP cells expressed BrdU (Fig. 4*F*; 62% in sham, $n = 3$ mice; 64% in MCAO, $n = 5$ mice; Mann–Whitney $U = 6$, $p = 0.786$), indicating that the majority of recorded RFP$^+$ neurons are born poststroke. The higher proportion of DCX$^+$ cells with a mature phenotype could also be caused by altered expression dynamics of DCX/RFP. If RFP expression were prolonged, one would expect a higher percentage of BrdU$^+$ cells expressing RFP. This was, however, not the case after MCAO (Fig. 4*G*; 70% in sham, $n = 3$ mice; 58.8%, $n = 5$ mice; Mann–Whitney $U = 5$, $p =$

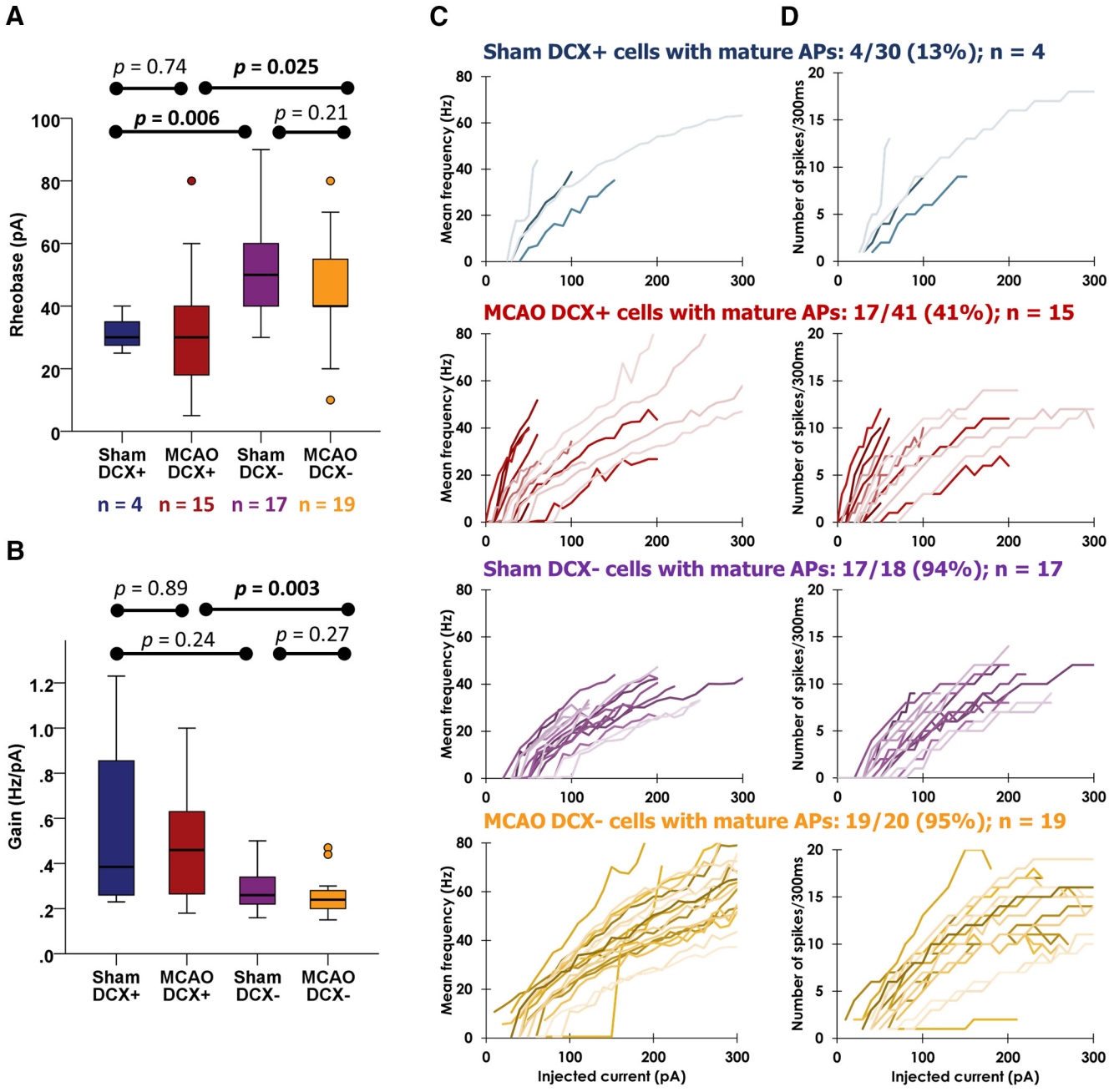

Figure 3. DCX$^+$ neurons with mature APs have an increased intrinsic excitability after stroke. Intrinsic excitability was analyzed only in those neurons showing mature action potentials (maximum dV/dt ≥ 300 V/s). ***A***, The rheobase (necessary current intensity to evoke an AP) of DCX$^+$ cells with mature APs was significantly lower than in their DCX$^-$ counterparts in both the sham and MCAO groups, but not within the DCX$^+$ or DCX$^-$ groups. ***B***, The mean output gain (mean slope of current–frequency curves) was significantly steeper in MCAO DCX$^+$ neurons with mature APs than in MCAO DCX$^-$ neurons. ***C***, ***D***, Individual input–output curves of recorded granule cells with mature APs are presented in as current-frequency (*I–V*; ***C***) curves and as the number of action potentials per current step (300 ms; ***D***). Each line represents the response of one neuron. The percentage of cells showing mature AP phenotype (AP rise slope > 300 V/s), and the number of cells (*n*) included in the analysis are presented above the figures. Two cells in the MCAO DCX$^+$ group were lost during recording. MCAO DCX$^+$ neurons show steeper curves in both output frequency and AP number compared with MCAO DCX$^-$ neurons ($p < 0.0001$ and 0.005, respectively), but also a higher output frequency compared with sham DCX$^+$ neurons ($p = 0.0004$). Mann–Whitney tests in ***A*** and ***B***, mixed linear models in ***C*** and ***D***. See text and Table 2 for statistical results. dV/dt = rise time of APs.

0.571). Therefore, most recorded RFP$^+$ neurons are born post-stroke, and there is no significant alteration in the expression of RFP after MCAO.

Glutamatergic synaptic input onto DCX$^+$ neurons is increased following stroke.

We next investigated the synaptic excitatory drive of DCX$^+$ neurons after stroke. We measured sEPSC, quantal currents (mEPSCs), and paired-pulse facilitation in response to LPP stimulation to evaluate excitatory synaptic input. sEPSC amplitude and frequency were highest in mature sham DCX$^-$ neurons and lowest in immature sham DCX$^+$ ABGCs (Table 3), as previously reported (Ye et al., 2005; Mongiat et al., 2009; Piatti et al., 2011; Schmidt-Salzmann et al., 2014). After MCAO, the amplitude of sEPSCs in DCX$^+$ ABGCs increased to levels similar to DCX$^-$ neurons (Fig. 5*A*,*B*; 7.4 pA; IQR, 2.5, $n = 12$; vs 5.3 pA; IQR, 2.3; $n = 6$ in MCAO DCX$^+$ and sham DCX$^+$ ABGCs, respectively; Mann–Whitney $U = 11$, $p = 0.018$), while the interevent interval

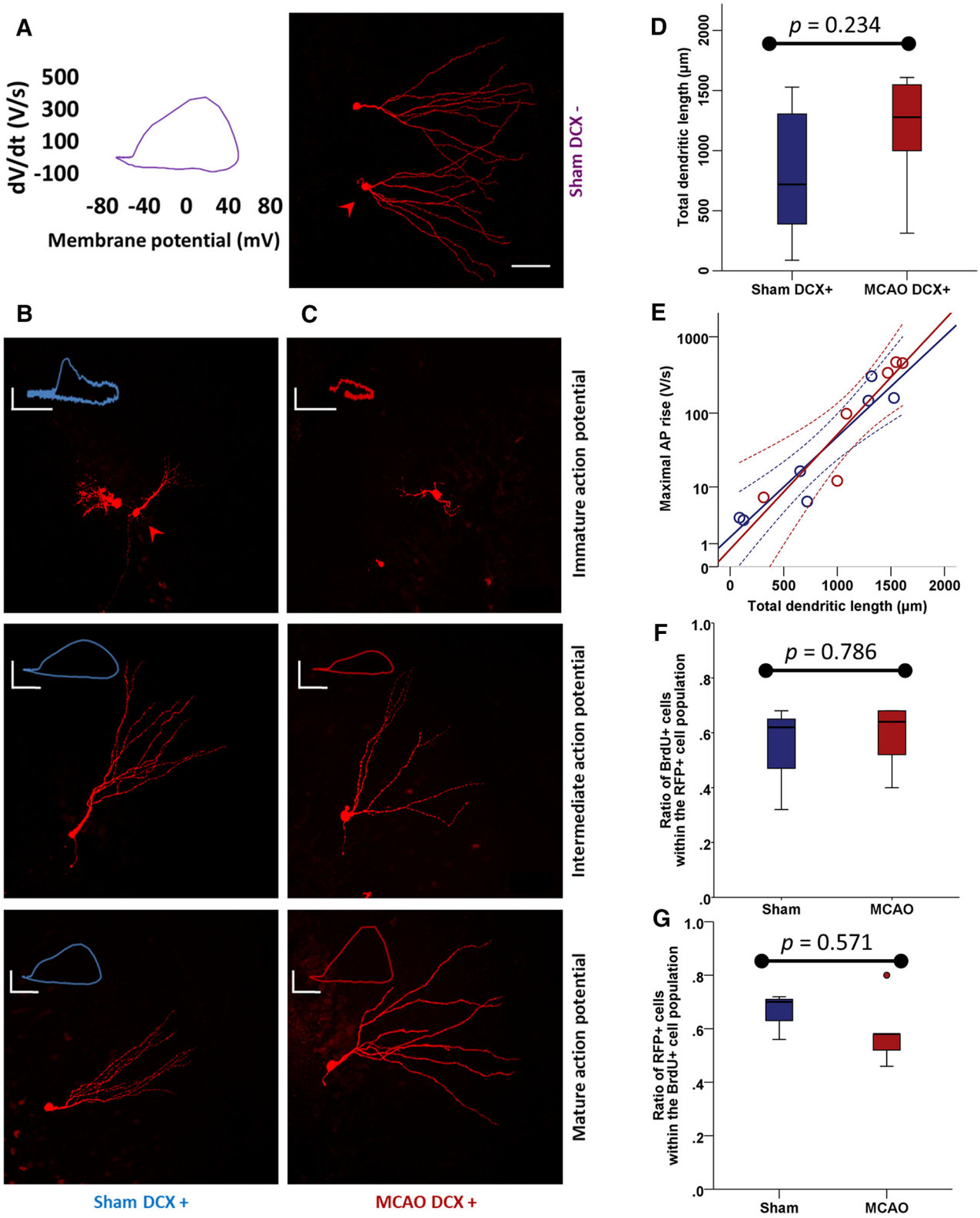

Figure 4. Conserved morphofunctional coordination in DCX $^{+}$ neurons after MCAO. ***A***, Right, Biocytin staining appearance of sham DCX $^{-}$ neurons shows an extensive, broad dendritic tree. Left, These cells have fast AP rise velocities. ***B***, ***C***, Morphological maturation follows maturation of intrinsic excitability in both sham DCX $^{+}$ (***B***) and MCAO DCX $^{+}$ (***C***) neurons (arrowheads indicate cells whose phase plots are represented. Scale bars, 50 μm. Calibration: immature AP, 20 mV, 10 V/s; intermediate AP, 30 mV, 50 V/s; mature AP, 20 mV, 200 V/s. ***D***, Dendritic morphology quantified as TDL by Sholl analysis did not change significantly in DCX $^{+}$ ABGCs ($n = 7$) after MCAO ($n = 6$). ***E***, A high level of correlation between morphological maturation (TDL) and functional maturation (maximal AP rise) was present in sham DCX $^{+}$ ABGCs and maintained after MCAO. ***F***, The proportion of BrdU $^{+}$ (born after the insult) cells within the RFP $^{+}$ cell population (a marker under the control of the DCX $^{-}$ promoter) does not change after MCAO and lies at ~60% ($n = 3$ in sham and $n = 5$ in MCAO groups). ***G***, The proportion of RFP $^{+}$ cells within the BrdU $^{+}$ subpopulation does not change, indicating conserved expression dynamics of RFP protein and hence DCX.

Table 3. Excitatory synaptic properties of hippocampal granule cells

	Sham DCX$^+$		Sham DCX$^-$		MCAO DCX$^+$		MCAO DCX$^-$		M-W *U* test Sham DCX$^+$ vs MCAO DCX$^+$			M-W *U* test Sham DCX$^-$ vs MCAO DCX$^-$		
Synaptic properties	*n/N*	Median (IQR)	*n/N*	Median (IQR)	*n/N*	Median (IQR)	*n/N*	Median (IQR)	*p*	*U*	η^2	*p*	*U*	η^2
sEPSC amplitude (pA)	6/5	5.3 (2.3)	6/3	8.5 (2.7)	12/9	7.4 (2.5)	17/5	7.2 (1.3)	0.018	11	32.2%	0.256	34	6.4%
sEPSC IEI (ms)		3084 (2605)		673 (1216)		1626 (4381)		1489 (1706)	0.75	32	0.8%	0.052	23	17.5%
mEPSC amplitude (pA)	6/4	5.1 (1.8)	6/3	6.3 (1.5)	9/7	8.0 (2.3)	15/5	6.4 (2.3)	0.002	2	62.0%	0.569	37	1.9%
mEPSC IEI (ms)		1742 (4274)		734 (716)		1403 (1839)		1546 (2079)	0.328	18	8.0%	0.008	12	33.0%
LPP facilitation	7/6	1.57 (1.05)			16/7	1.53 (1.36)			0.076	29	14.8%			
In cells with mature AP									Sham DCX$^-$ vs MCAO DCX$^+$			Sham DCX$^-$ vs MCAO DCX$^-$		
sEPSC amplitude (pA)			6/3	8.5 (2.7)	7/6	7.6 (2.3)	16/5	7.2 (1.0)	0.445	15	6.1%	0.231	31	7.5%
sEPSC IEI (ms)				673 (1216)		1495 (848)		1496 (1756)	0.138	10	20.6%	0.049	21	18.9%
mEPSC amplitude (pA)			6/3	6.3 (1.5)	6/5	8.1 (1.0)	14/5	6.4 (2.3)	0.009	2	59.7%	0.718	37	0.9%
mEPSC IEI (ms)				734 (716)		1418 (1753)		1421 (2239)	0.310	11	11.4%	0.012	12	32.2%

M-W, Mann–Whitney; *n/N* = number of cells/number of mice. Summary of excitatory synaptic properties in the four recorded groups. sEPSCs were measured with 10 μM PTX added in the bath solution, while mEPSCs with 10 μM PTX and 1 μM TTX in the bath solution. The statistical unit is *n*.

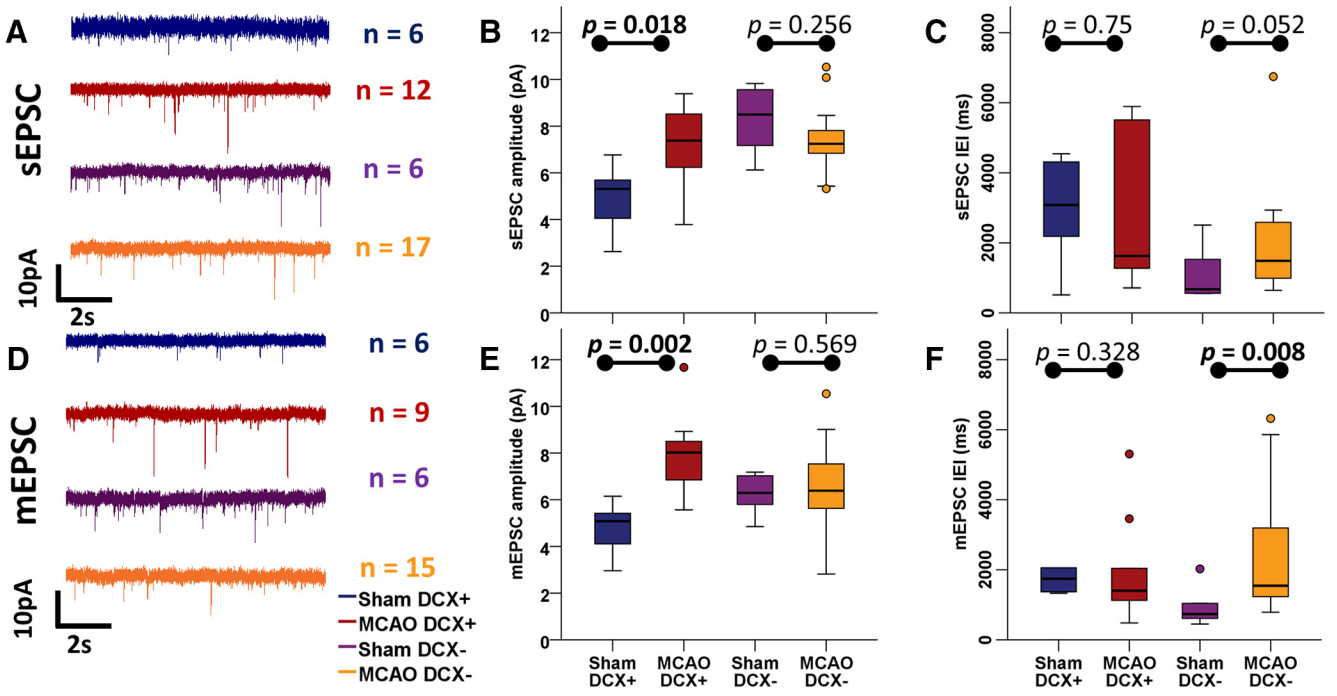

Figure 5. Glutamatergic synaptic input onto DCX$^+$ neurons is increased following stroke. ***A***, Representative traces of sEPSC input (recorded at −82 mV in the presence of 10 μM PTX) onto granule cells. ***B***, ***C***, Distribution of sEPSC amplitudes (***B***) and IEIs (***C***) onto granule cells. DCX$^+$ neurons show significantly increased sEPSC amplitudes, and no change in IEI after MCAO, whereas sEPSC input onto DCX$^-$ neurons does not change in either amplitude or IEI following MCAO. ***D***, Representative traces of mEPSC input (recorded at −82 mV in the presence of 10 μM PTX and 1 μM TTX) onto granule cells. ***E***, ***F***, Distribution of mEPSC amplitudes (***E***) and IEIs (***F***) of granule cells. DCX$^+$ neurons show significantly increased mEPSC amplitudes, and no change in frequencies after MCAO, whereas mEPSC frequency decreases (IEI increases) in DCX$^-$ neurons following MCAO. See also Table 3 for statistical results.

(IEI) remained unchanged (Fig. 5*A*,*C*, Table 3). These changes were specific for DCX$^+$ neurons, since MCAO did not affect sEPSC amplitude or IEI in DCX$^-$ neurons. Analyzing quantal events, we also found a significant increase in the amplitude of mEPSC following MCAO in DCX$^+$ neurons (Fig. 5*D*,*E*; 8 pA; IQR, 2.3; $n = 9$; vs 5.1 pA; IQR, 1.8; $n = 6$ in MCAO DCX$^+$ and sham DCX$^+$ ABGCs, respectively; Mann–Whitney $U = 2$, $p = 0.002$), while IEI remained unaltered (Fig. 5*D*,*F*, Table 3). Paired-pulse stimulation of the LPP (100 ms intervals) resulted in a facilitation of the second response in both sham and MCAO DCX$^+$ cells. LPP facilitation in DCX$^+$ ABGCs was not changed after ischemia (Table 3; Mann–Whitney $U = 5299.5$, $p = 0.63$), corroborating the analysis of mEPSC and indicating an unaltered, low probability of release of presynaptic boutons targeting DCX$^+$ ABGCs. Furthermore, these observations were also present in MCAO DCX$^+$ neurons with mature APs, whose sEPSC and mEPSC amplitudes reached or exceeded the levels of normally integrated sham DCX$^-$ neurons (Table 3).

These data suggest that postischemic, intrinsically hyperexcitable DCX$^+$ neurons integrate in the dentate gyrus network and receive large excitatory currents most likely mediated by postsynaptic changes (e.g., by increased sensitivity to released glutamate or AMPA receptor recruitment).

Uncoupled intrinsic and synaptic excitability in DCX$^+$ ABGCs after stroke

Both intrinsic excitability and excitatory synaptic input evolve during physiological granule cell development. We sought to determine whether the stroke-induced accelerated maturation of the above-mentioned parameters follows physiological dynamics. We therefore tested whether a marker of intrinsic development (R_{input}) correlated with a marker of synaptic development

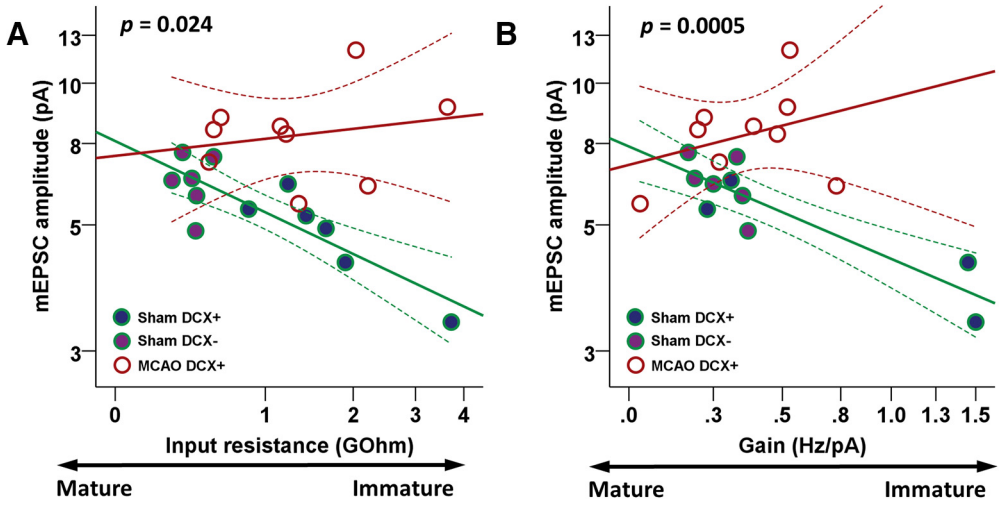

Figure 6. Uncoupled intrinsic and synaptic excitability in DCX$^+$ ABGCs after stroke. ***A***, Input resistance, a parameter of passive neuronal properties, was plotted against mEPSC amplitude, a parameter of synaptic excitability. Sham DCX$^+$ and sham DCX$^-$ neurons were grouped together, representing the continuum of physiologically developed neurons. Regression lines (full lines) and the 95% confidence interval of the mean (dashed lines) were fitted to the data. mEPSC amplitude increases with maturation, as R_{input} decreases in sham DCX$^+$/DCX$^-$ cells ($R^2 = 0.719$). This relationship is lost after MCAO ($R^2 = 0.041$), with immature cells receiving disproportionately large excitatory synaptic currents. Statistical analysis by GLM showed a significant difference in the evolution of the two parameters between the two groups ($n = 12$ sham DCX$^+$/DCX$^-$, $n = 9$ MCAO DCX$^+$; $F_{(1,17)} = 6.1$, $p = 0.024$). ***B***, Output gain, a parameter of intrinsic excitability, was plotted against mEPSC amplitude, a parameter of synaptic excitability, under the same conditions as in ***A***. Sham DCX$^+$/DCX$^-$ neurons have a progressive increase in synaptic excitability, which is accompanied by a decrease in output gain ($R^2 = 0.783$), thus preserving a balance between intrinsic and synaptic excitability. MCAO DCX$^+$ show a dysregulated development of intrinsic and synaptic excitability ($R^2 = 0.115$), with highly excitable, immature neurons receiving disproportionately strong excitatory inputs. Statistical analysis revealed here as well a significant difference in the evolution of the two parameters in sham and MCAO groups ($n = 12$ sham DCX$^+$/DCX$^-$, $n = 9$ MCAO DCX$^+$; $F_{(1,15)} = 19.6$, $p = 0.0005$).

(mEPSC amplitude). Furthermore, we analyzed whether a marker of intrinsic excitability (mean output gain) correlated with the same marker of synaptic development (mEPSC amplitude). We used the GLM to test for statistical significance, and, since all three parameters followed non-normal distributions, we used the logarithm-transformed data.

Since sham DCX$^+$ and sham DCX$^-$ neurons represent the physiological continuum of the development of hippocampal granule cells, these cells were pooled together in the group sham DCX$^+$/DCX$^-$. There was a highly correlated development of passive maturation (R_{input}) and synaptic excitability (mEPSC amplitude) in sham DCX$^+$/DCX$^-$ cells ($R^2 = 0.719$, $n = 12$; Fig. 6*A*), pointing to a tightly coupled intrinsic and network maturation. After ischemia, this correlation was lost in DCX$^+$ ABGCs ($R^2 = 0.041$), resulting in immature cells with high R_{input} receiving disproportionately large excitatory inputs ($n = 12$ sham DCX$^+$/DCX$^-$, $n = 9$ MCAO DCX$^+$; $F_{(1,17)} = 6.1$, $p = 0.024$). Intrinsic excitability (mean output gain) was also tightly coupled to synaptic excitability (mEPSC amplitude, $R^2 = 0.783$; Fig. 6*B*), with lower mEPSC amplitudes compensating for a higher gain in physiologically developed sham DCX$^+$/DCX$^-$ neurons. This correlation was again lost after ischemia in DCX$^+$ ABGCs ($R^2 = 0.115$; $n = 12$ sham DCX$^+$/DCX$^-$, $n = 9$ MCAO DCX$^+$; $F_{(1,15)} = 19.6$, $p = 0.0005$). Intrinsically hyperexcitable, high-gain MCAO DCX$^+$ neurons received disproportionately large synaptic excitation. We found similar results when analyzing correlated development between only the sham DCX$^+$ and MCAO$^+$ neurons (data not shown). Thus, the maturation of DCX$^+$ ABGCs following stroke is characterized by uncoupled dynamics in intrinsic and synaptic maturation. Subsequently, high-R_{input} and high-output gain cells are not counterbalanced by lower afferent excitation, resulting in MCAO DCX$^+$ cells that are potentiated by a higher excitatory input.

Discussion

Stroke causes an increase in adult hippocampal neurogenesis, but the functional relevance of more ABGCs is uncertain. While under physiological conditions higher rates of neurogenesis and increased number of cells in the dentate gyrus may improve cognition (Sahay et al., 2011), the same may not necessarily be true under a pathological environment. Under the above assumption, increased numbers of morphologically normal ABGCs poststroke should undergo physiological maturation and integrate normally in the dentate gyrus to provide a functional benefit. However, mice showed an aggravation of memory deficits when neurogenesis was further increased (by running) after stroke (Woitke et al., 2017). Previous morphological studies point toward impaired neurogenesis after stroke by demonstrating aberrant cell development, although the majority of ABGCs express normal morphology with typical dendritic arborization and synapse formation poststroke (Niv et al., 2012). Based on these previous observations, we here addressed the important questions if these newly generated neurons are functional and integrate in the hippocampal network. Moreover, we investigated whether these neurons contribute to a physiological function and constitute a beneficial element for the network.

The hyperexcitability of immature ABGCs in the first month after birth compared with resident granule cells is well documented under physiological conditions (Schmidt-Hieber et al., 2004; Couillard-Després et al., 2006; Mongiat et al., 2009; Brunner et al., 2014; Dieni et al., 2016). We here show an increase in the number of such hyperexcitable, young ABGCs after stroke through accelerated maturation. The electrotonic properties of these neurons reach values closer to those of mature DCX$^-$ neurons, thus indicating a process of accelerated maturation, which adds to the already enhanced process of neurogenesis. Furthermore, a higher proportion of DCX$^+$ ABGCs in the postischemic hippocampus can fire mature action potentials (i.e., with rates of

rise >300 V/s) and at a higher gain than DCX$^-$ neurons. These effects are specific for DCX$^+$ cells, since DCX$^-$ neurons are differently affected.

Evidence of network integration of postischemic DCX$^+$ ABGCs is provided by the detection of spontaneous excitatory synaptic currents. sEPSCs are larger in DCX$^+$ ABGCs following stroke, mediated by a higher postsynaptic potency of glutamate, as inferred from larger mEPSC amplitudes but unchanged mEPSC frequencies and unchanged release probability. Sham DCX$^-$ neurons, on the other hand, were again differently affected by stroke and showed only a decrease in the frequency of quantal excitatory events, pointing to a presynaptic expression pattern, while sEPSC and mEPSC amplitudes remained unchanged.

Accelerated intrinsic maturation and action potential generation does not necessarily preclude normal function. As mentioned above, young, spiking ABGCs are physiologically more excitable, with higher output gain, presumably to compensate for a lower synaptic drive (Mongiat et al., 2009; Brunner et al., 2014). We found similar features of hyperexcitability in DCX$^+$ ABGCs after stroke, but in a substantially higher number of cells.

An increase in sEPSC/mEPSC amplitudes following stroke might be normal if it were proportional to the developmental stage of the neurons. In clear contrast to the physiological developmental dynamics with coupled and highly correlated development of electrotonic and intrinsic excitability with excitatory synaptic input, postischemic DCX$^+$ ABGCs show an uncoupled, aberrant development. This results in hyperexcitable (high-R_{input}, high gain) ABGCs receiving high-amplitude glutamatergic input, whereas under physiological maturation the hyperexcitability of immature neurons is compensated for by a lower excitatory synaptic drive. Therefore, our results argue not only for an accelerated maturation, but for an aberrant development of DCX$^+$ ABGCs poststroke.

Stroke is not the only pathological stimulus that results in a disruption of adult neurogenesis in the hippocampus. The degree of damage and its functional consequences seem to be dependent on the underlying pathological event (e.g., after epileptic, ischemic, traumatic, or inflammatory lesions). The steps of cellular maturation and functional integration after a lesion appear to develop in a pathology-specific manner. Profound morphological alterations after experimental traumatic brain injury, for example, do not preclude physiological development and integration of ABGCs in this pathological environment (Villasana et al., 2015). However, after status epilepticus induced by local electrical stimulation, ABGCs showed reduced network excitatory drive, which is driven presynaptically by a reduced release probability (Jakubs et al., 2006). In contrast to this and similar to our findings, in a model of pilocarpine-induced status epilepticus, immature neurons showed an accelerated intrinsic maturation and also premature development of excitatory synaptic drive, including recurrent polysynaptic inputs (Overstreet-Wadiche et al., 2006). Thus, the environment in which ABGCs mature is fundamental to the development of new cells, and the pathological environment drives different responses regarding maturation and integration of ABGCs (Wood et al., 2011). Whether newborn cells in a pathological environment provide a functional benefit or represent a maladaptive response may also be condition specific (Surget et al., 2011; Hester and Danzer, 2013; Hosford et al., 2016).

In conclusion, our results provide evidence that morphologically normal DCX$^+$ ABGCs following stroke show faster maturation to become operative and integrated in the hippocampal network. However, the functional development of these cells is aberrant, resulting in an uncoupled synaptic hyperexcitability potentiating the intrinsic hyperexcitability of DCX$^+$ ABGCs even at 2 weeks following the injury. Finally, to unequivocally determine whether this increased excitability is a cause rather than a consequence of hippocampal dysfunction, further studies correlating cellular and network function to behavioral outcome while modulating neurogenesis will be needed to unequivocally show the effect of increased neurogenesis on memory function and seizure susceptibility.

References

Adlaf EW, Vaden RJ, Niver AJ, Manuel AF, Onyilo VC, Araujo MT, Dieni CV, Vo HT, King GD, Wadiche JI, Overstreet-Wadiche L (2017) Adult-born neurons modify excitatory synaptic transmission to existing neurons. Elife 6:e19886. CrossRef Medline

Ambrogini P, Cuppini R, Lattanzi D, Ciuffoli S, Frontini A, Fanelli M (2010) Synaptogenesis in adult-generated hippocampal granule cells is affected by behavioral experiences. Hippocampus 20:799–810. CrossRef Medline

Arvidsson A, Kokaia Z, Lindvall O (2001) N-methyl-D-aspartate receptor-mediated increase of neurogenesis in adult rat dentate gyrus following stroke. Eur J Neurosci 14:10–18. CrossRef Medline

Benjamini Y, Drai D, Elmer G, Kafkafi N, Golani I (2001) Controlling the false discovery rate in behavior genetics research. Behav Brain Res 125:279–284. CrossRef Medline

Bergami M, Masserdotti G, Temprana SG, Motori E, Eriksson TM, Göbel J, Yang SM, Conzelmann KK, Schinder AF, Götz M, Berninger B (2015) A critical period for experience-dependent remodeling of adult-born neuron connectivity. Neuron 85:710–717. CrossRef Medline

Brown JP, Couillard-Després S, Cooper-Kuhn CM, Winkler J, Aigner L, Kuhn HG (2003) Transient expression of doublecortin during adult neurogenesis. J Comp Neurol 467:1–10. CrossRef Medline

Brunner J, Neubrandt M, Van-Weert S, Andrási T, Kleine Borgmann FB, Jessberger S, Szabadics J (2014) Adult-born granule cells mature through two functionally distinct states. Elife 3:e03104. CrossRef Medline

Chugh D, Nilsson P, Afjei SA, Bakochi A, Ekdahl CT (2013) Brain inflammation induces post-synaptic changes during early synapse formation in adult-born hippocampal neurons. Exp Neurol 250:176–188. CrossRef Medline

Couillard-Després S (2013) Hippocampal neurogenesis and ageing. Curr Top Behav Neurosci 15:343–355. CrossRef Medline

Couillard-Despres S, Winner B, Schaubeck S, Aigner R, Vroemen M, Weidner N, Bogdahn U, Winkler J, Kuhn HG, Aigner L (2005) Doublecortin expression levels in adult brain reflect neurogenesis. Eur J Neurosci 21:1–14. CrossRef Medline

Couillard-Despres S, Winner B, Karl C, Lindemann G, Schmid P, Aigner R, Laemke J, Bogdahn U, Winkler J, Bischofberger J, Aigner L (2006) Targeted transgene expression in neuronal precursors: watching young neurons in the old brain. Eur J Neurosci 24:1535–1545. CrossRef Medline

Dieni CV, Panichi R, Aimone JB, Kuo CT, Wadiche JI, Overstreet-Wadiche L (2016) Low excitatory innervation balances high intrinsic excitability of immature dentate neurons. Nat Commun 7:11313. CrossRef Medline

Hester MS, Danzer SC (2013) Accumulation of abnormal adult-generated hippocampal granule cells predicts seizure frequency and severity. J Neurosci 33:8926–8936. CrossRef Medline

Hosford BE, Liska JP, Danzer SC (2016) Ablation of newly generated hippocampal granule cells has disease-modifying effects in epilepsy. J Neurosci 36:11013–11023. CrossRef Medline

Ikrar T, Guo N, He K, Besnard A, Levinson S, Hill A, Lee HK, Hen R, Xu X, Sahay A (2013) Adult neurogenesis modifies excitability of the dentate gyrus. Front Neural Circuits 7:204. CrossRef Medline

Jagasia R, Steib K, Englberger E, Herold S, Faus-Kessler T, Saxe M, Gage FH, Song H, Lie DC (2009) GABA-cAMP response element-binding protein signaling regulates maturation and survival of newly generated neurons in the adult hippocampus. J Neurosci 29:7966–7977. CrossRef Medline

Jakubs K, Nanobashvili A, Bonde S, Ekdahl CT, Kokaia Z, Kokaia M, Lindvall O (2006) Environment matters: synaptic properties of neurons born in the epileptic adult brain develop to reduce excitability. Neuron 52:1047–1059. CrossRef Medline

Jakubs K, Bonde S, Iosif RE, Ekdahl CT, Kokaia Z, Kokaia M, Lindvall O

(2008) Inflammation regulates functional integration of neurons born in adult brain. J Neurosci 28:12477–12488. CrossRef Medline

Jessberger S, Zhao C, Toni N, Clemenson GD Jr, Li Y, Gage FH (2007) Seizure-associated, aberrant neurogenesis in adult rats characterized with retrovirus-mediated cell labeling. J Neurosci 27:9400–9407. CrossRef Medline

Karl C, Couillard-Despres S, Prang P, Munding M, Kilb W, Brigadski T, Plötz S, Mages W, Luhmann H, Winkler J, Bogdahn U, Aigner L (2005) Neuronal precursor-specific activity of a human doublecortin regulatory sequence. J Neurochem 92:264–282. CrossRef Medline

Kempermann G, Kuhn HG, Gage FH (1997) More hippocampal neurons in adult mice living in an enriched environment. Nature 386:493–495. CrossRef Medline

Kluska MM, Witte OW, Bolz J, Redecker C (2005) Neurogenesis in the adult dentate gyrus after cortical infarcts: effects of infarct location, N-methyl-D-aspartate receptor blockade and anti-inflammatory treatment. Neuroscience 135:723–735. CrossRef Medline

Liu J, Solway K, Messing RO, Sharp FR (1998) Increased neurogenesis in the dentate gyrus after transient global ischemia in gerbils. J Neurosci 18:7768–7778. CrossRef Medline

Liu X, Tilwalli S, Ye G, Lio PA, Pasternak JF, Trommer BL (2000) Morphologic and electrophysiologic maturation in developing dentate gyrus granule cells. Brain Res 856:202–212. CrossRef Medline

Loubinoux I, Kronenberg G, Endres M, Schumann-Bard P, Freret T, Filipkowski RK, Kaczmarek L, Popa-Wagner A (2012) Post-stroke depression: mechanisms, translation and therapy. J Cell Mol Med 16:1961–1969. CrossRef Medline

Mijajlovic MD, Pavlović A, Brainin M, Heiss WD, Quinn TJ, Ihle-Hansen HB, Hermann DM, Assayag EB, Richard E, Thiel A, Kliper E, Shin YI, Kim YH, Choi S, Jung S, Lee YB, Sinanović O, Levine DA, Schlesinger I, Mead G, et al (2017) Post-stroke dementia-a comprehensive review. BMC Med 15:11. CrossRef Medline

Mongiat LA, Espósito MS, Lombardi G, Schinder AF (2009) Reliable activation of immature neurons in the adult hippocampus. PLoS One 4:e5320. CrossRef Medline

Nakashiba T, Cushman JD, Pelkey KA, Renaudineau S, Buhl DL, McHugh TJ, Rodriguez Barrera V, Chittajallu R, Iwamoto KS, McBain CJ, Fanselow MS, Tonegawa S (2012) Young dentate granule cells mediate pattern separation, whereas old granule cells facilitate pattern completion. Cell 149:188–201. CrossRef Medline

Niv F, Keiner S, Krishna-Witte OW, Lie DC, Redecker C (2012) Aberrant neurogenesis after stroke: a retroviral cell labeling study. Stroke 43:2468–2475. CrossRef Medline

Nokia MS, Sisti HM, Choksi MR, Shors TJ (2012) Learning to learn: theta oscillations predict new learning, which enhances related learning and neurogenesis. PLoS One 7:e31375. CrossRef Medline

Overstreet-Wadiche LS, Bromberg DA, Bensen AL, Westbrook GL (2006) Seizures accelerate functional integration of adult-generated granule cells. J Neurosci 26:4095–4103. CrossRef Medline

Piatti VC, Davies-Sala MG, Espósito MS, Mongiat LA, Trinchero MF, Schinder AF (2011) The timing for neuronal maturation in the adult hippocampus is modulated by local network activity. J Neurosci 31:7715–7728. CrossRef Medline

Robinson RG, Jorge RE (2016) Post-stroke depression: a review. Am J Psychiatry 173:221–231. CrossRef Medline

Sahay A, Scobie KN, Hill AS, O'Carroll CM, Kheirbek MA, Burghardt NS, Fenton AA, Dranovsky A, Hen R (2011) Increasing adult hippocampal neurogenesis is sufficient to improve pattern separation. Nature 472:466–470. CrossRef Medline

Schmidt-Hieber C, Jonas P, Bischofberger J (2004) Enhanced synaptic plasticity in newly generated granule cells of the adult hippocampus. Nature 429:184–187. CrossRef Medline

Schmidt-Salzmann C, Li L, Bischofberger J (2014) Functional properties of extrasynaptic AMPA and NMDA receptors during postnatal hippocampal neurogenesis. J Physiol 592:125–140. CrossRef Medline

Spampanato J, Sullivan RK, Turpin FR, Bartlett PF, Sah P (2012) Properties of doublecortin expressing neurons in the adult mouse dentate gyrus. PLoS One 7:e41029. CrossRef Medline

Surget A, Tanti A, Leonardo ED, Laugeray A, Rainer Q, Touma C, Palme R, Griebel G, Ibarguen-Vargas Y, Hen R, Belzung C (2011) Antidepressants recruit new neurons to improve stress response regulation. Mol Psychiatry 16:1177–1188. CrossRef Medline

van Praag H, Kempermann G, Gage FH (1999) Running increases cell proliferation and neurogenesis in the adult mouse dentate gyrus. Nat Neurosci 2:266–270. CrossRef Medline

van Praag H, Schinder AF, Christie BR, Toni N, Palmer TD, Gage FH (2002) Functional neurogenesis in the adult hippocampus. Nature 415:1030–1034. CrossRef Medline

Villasana LE, Kim KN, Westbrook GL, Schnell E (2015) Functional integration of adult-born hippocampal neurons after traumatic brain injury(1,2,3). eNeuro 2: ENEURO.0056-15.2015. CrossRef Medline

Walter J, Keiner S, Witte OW, Redecker C (2011) Age-related effects on hippocampal precursor cell subpopulations and neurogenesis. Neurobiol Aging 32:1906–1914. CrossRef Medline

Wang SH, Zhang ZJ, Guo YJ, Sui YX, Sun Y (2010) Involvement of serotonin neurotransmission in hippocampal neurogenesis and behavioral responses in a rat model of post-stroke depression. Pharmacol Biochem Behav 95:129–137. CrossRef Medline

Woitke F, Ceanga M, Rudolph M, Niv F, Witte OW, Redecker C, Kunze A, Keiner S (2017) Adult hippocampal neurogenesis poststroke: more new granule cells but aberrant morphology and impaired spatial memory. PLoS One 12:e0183463. CrossRef Medline

Wood JC, Jackson JS, Jakubs K, Chapman KZ, Ekdahl CT, Kokaia Z, Kokaia M, Lindvall O (2011) Functional integration of new hippocampal neurons following insults to the adult brain is determined by characteristics of pathological environment. Exp Neurol 229:484–493. CrossRef Medline

Ye GL, Yi S, Gamkrelidze G, Pasternak JF, Trommer BL (2005) AMPA and NMDA receptor-mediated currents in developing dentate gyrus granule cells. Brain Res Dev Brain Res 155:26–32. CrossRef Medline

Zhao C, Deng W, Gage FH (2008) Mechanisms and functional implications of adult neurogenesis. Cell 132:645–660. CrossRef Medline